Research in Astronomy and Astrophysics, 23:075013 (10pp), 2023 July https://doi.org/10.1088/1674-4527/acd52d

First Detailed Photometric Investigation on the Nature of Contact Binary System AA Cet

M. F. Yıldırım[1] and F. Soydugan[1,2]
[1] Çanakkale Onsekiz Mart University, Astrophysics Research Center and Ulupınar Observatory, 17020, Çanakkale, Turkey; mf.yildirim@hotmail.com
[2] Çanakkale Onsekiz Mart University, Faculty of Sciences, Department of Physics, 17020, Çanakkale, Turkey
Received 2023 January 28; revised 2023 April 12; accepted 2023 April 26; published 2023 June 15

Abstract

The TESS light curve (LC) of the marginal contact binary AA Cet was analyzed simultaneously with the radial velocity and the orbital period (OP) change of the system was investigated. The physical parameters of the system were obtained by analyzing the LC of AA Cet with the Wilson-Devinney method, and the absolute parameters of the components were calculated using the results obtained. For the components of AA Cet, the masses and radii were calculated as $M_1 = 1.39 \pm 0.04\ M_\odot$, $M_2 = 0.48 \pm 0.02\ M_\odot$ and $R_1 = 1.64 \pm 0.03\ R_\odot$, $R_2 = 1.01 \pm 0.04\ R_\odot$, respectively. AA Cet is a marginal contact binary with a temperature difference of 1305 K between its components. A total of 14 eclipse times were obtained from the TESS data and used in the OP analysis together with those collected from the literature. It has been observed that the change in the OP of AA Cet is in the form of a decreasing parabola. Conservative mass transfer between the components has been interpreted as the reason for this change. The OP decrease amount of AA Cet was obtained as $dP/dt = 0.0062 \pm 0.0006$ s yr^{-1}, and the reason for this decrease was attributed to a $3.3(9) \times 10^{-8}\ M_\odot$ mass transfer per year from the more massive component to the less massive one. The age of AA Cet has been estimated as 7 Gyr, as the age of contact systems helps us to understand their evolution.

Key words: (stars:) binaries: eclipsing – stars: fundamental parameters – stars: individual (AA Cet)

1. Introduction

Because contact binaries (CBs) are encircled by a common envelope, the surface temperatures of the components are almost the same. However, for some CB systems (e.g., AA Cet), the temperature difference between the components is quite large. Many authors (e.g., Flannery 1976; Lucy 1976; Qian 2001a, 2001b, 2003) have attempted to explain this situation with thermal relaxation oscillation (TRO). Binnendijk (1970) categorized CBs into A and W-type subclasses. For eclipsing binaries (EBs), the most easily determined parameter is the orbital period (OP). A subclass of EBs, the CBs, usually have OPs of less than one day. A statistical study on 700 CBs was conducted by Latkovic et al. (2021). They reported that the OPs of such systems were mostly shorter than 0.5 day. A correlation between the OP and the masses of the components was determined by Gazeas & Stepien (2008) using 112 CBs. The relationship between $M-R$ and $M-L$ for the CBs was obtained by Zhang et al. (2020). The reason why the second components of the A and W types are overluminous is due to the fact that the second components for A types have evolved from more massive stars, while the W types are due to energy transfer (Zhang et al. 2020). Thanks to these correlations obtained from such studies in the literature, general inferences can be drawn about CBs. By determining the basic astrophysical parameters of binary stars, information about the evolution of the systems can be obtained. Therefore, the marginal contact AA Cet, whose basic astrophysical parameters are unknown, was chosen, and its basic astrophysical parameters were calculated.

The difference between eclipses of the marginal CB AA Cet (HD 12180, ADS 1581 A, TIC 266769522, Gaia DR3 5134682575449602560, SAO 167451, TYC 6430−631−1) is quite large, and the OP of AA Cet is about half a day. AA Cet was discovered by Bloomer (1971a) as a variable system, and light elements were reported by Bloomer (1971b). The light elements for AA Cet were updated by Bloomer (1972) as $T_o = 2441268.6869(7)$ and $P = 0.53617353(50)$, and calculated differently from Bloomer (1971b). The study of a new quadruple star system was done by Chambliss (1981). In the same study, it was reported that the visual binary was composed of an AA Cet member with SAO 167451 and another member with SAO 167450. SAO 167450: It was stated by Chambliss (1981) that it is a double-lined spectroscopic binary, but eclipses are not observed. (Radial velocity (RV) values are calculated as $-12(2)$ km s^{-1} and $+68(1)$ km s^{-1}.) The spectral type of AA Cet (SAO 167451) was determined as F2 and the spectral type of SAO 167450 as F5 by Chambliss (1981). The RV curve analysis of AA Cet was made by Duerbeck & Rucinski (2007), and they determined the mass ratio of AA Cet to be $q = 0.35(2)$. In addition, the RV study of the system was also done by Pribulla et al. (2009), and the spectral type of AA Cet was determined as F4V. A study of the other member of the visual binary, SAO 167450, was performed by Fekel & Willmarth (2009). They also reported that the system is quadruple. There is no photometric analysis study on AA Cet in the literature. For this reason, AA Cet was selected in this study, and photometric analysis was performed for the first time.

2. Data Information

Photometric observations of the visual binary AA Cet were made by the TESS satellite (Ricker et al. 2015). Photometric observation data were archived by MAST.[3] TESS observations for AA Cet were made for about a month in 2018 (starting on the 20th of September and completed on the 17th of October). In addition, a one-month observation was made in 2020, which started on September 23 and was completed on October 20. While the exposure time of the 2018 observation was 120 s, the exposure time of the 2020 observation was 600 s (sequence numbers: 3 and 30, respectively). The light curves (LCs) of TESS data are in Barycentric Julian Date (BJD), but data in the literature are usually in Heliocentric Julian Date (HJD), so the data were transformed from BJD into HJD. The eclipse times were calculated from the LC data using a code based on the least squares method. Eclipse times for OP analysis were taken from the $O - C$ gateway (Paschke & Brat 2006) and listed in Table 1 along with those calculated from the TESS data.

3. The Light Curve Modeling

Since the LC analysis of AA Cet has not been done yet, it is aimed to model the sensitive TESS LC data of the system. For analysis, the van Hamme & Wilson (2003) version of the Wilson-Devinney (WD, Wilson & Devinney 1971) code was preferred. While performing the LC analysis, the analysis was first conducted in Mode 2 for detached binaries. During the analysis, it was observed that both components filled their Roche lobes. After that, Mode 3 was chosen for the CBs, where both components filled their Roche lobes. The spectral type of AA Cet was determined as F4V by Pribulla et al. (2009), and the temperature of the first component was taken as 6500 K, as recommended by Eker et al. (2020) according to this spectral type. The gravitational darkening coefficients and the bolometric albedo coefficients were taken as $g_1 = g_2 = 0.32$ (Lucy 1967) and $A_1 = A_2 = 0.5$ (Rucinski 1969), respectively, with the assumption of a convective atmosphere. The logarithmic edge-darkening coefficients given by van Hamme (1993) were used. In the LC analysis for AA Cet, the analysis was started with the initial mass ratio value reported by Duerbeck & Rucinski (2007). The LC of AA Cet was analyzed simultaneously with the RV data obtained by Duerbeck & Rucinski (2007) and archived in the SB9 database[4] by Pourbaix et al. (2004). Correction amounts and errors were calculated for the free parameters using the differential correction (DC) method in the WD program. (The free parameters in the analysis, along with their errors, are listed in Table 2.) In iterations, if the correction amounts of the free parameters are smaller than the errors, the solution is reached. The parameters derived from the LC analysis are listed in Table 2, and the compatibility between the observational data and the theoretical fit in the LC graph is illustrated in Figure 1. A comparison of the observational RV data with the theoretical fit obtained from the analysis is also depicted in Figure 2.

4. The Orbital Period Variation

It is very important to examine the OP changes of binary systems in terms of providing information about their structures and evolutions. OP changes can be in the form of an increase or decrease in the period. Mass and angular momentum transfers change the OP of AA Cet. To determine the OP change, the $O - C$ graph is created by taking the difference between the observed (O) and calculated (C) eclipse times. If there is a change in the OP of the system, it will be observed in the $O - C$ graph as a form of an up or down parabolic change. $O - C$ gateway (Paschke & Brat 2006) and Atlas $O - C$ (Kreiner 2004) databases were used first, since the OP analysis of AA Cet has not been performed so far. It was seen from both data archives that the OP of AA Cet decreased; the light elements of AA Cet are expressed in Equations (1) and (2) for the $O - C$ gateway and Atlas $O - C$, respectively.

$$\mathrm{MinI(HJD)} = 2441268.689 + 0.536169 \times E. \tag{1}$$

$$\mathrm{MinI(HJD)} = 2441268.6915 + 0.536169082 \times E. \tag{2}$$

In these equations, E represents the number of cycles. In the $O - C$ analysis, these light elements were chosen as initial values. As a result of the analysis, light elements and errors in Equation (3) were obtained.

$$\mathrm{MinI(HJD)} = 2448500.0096(5) + 0.5361691(7) \times E. \tag{3}$$

Since AA Cet is a CB, mass transfer between components may cause an $O - C$ variation. If the mass transfer is large enough, a parabolic $O - C$ change will be observed. The OP change analysis was performed with a total of 264 eclipse times (14 eclipse times calculated from TESS data in this study), and it was seen that the OP of AA Cet decreased with time (see Figure 3). A differential correction method was applied to obtain the light elements and quadratic term in Equation (4) using the eclipse times in Table 1.

$$\mathrm{MinI(HJD)} = 2448500.0096(5) + 0.5361691(7) \times E - 0.53(5) \times 10^{-10} \times E^2. \tag{4}$$

[3] MAST, https://archive.stsci.edu.

[4] SB9 database, http://sb9.astro.ulb.ac.be.

Table 1
The Eclipse Times used in the Orbital Period Analysis for AA Cet (The $O-C$ values were Calculated using Equation (4))

HJD (2400000+)	Type	Method	Epoch	$O-C$ (d)	References
38369.3130	s	pg	−18,894.5	−0.0495	IBVS No.587
38728.3190	p	pg	−18,225	−0.0087	IBVS No.587
38995.5940	s	pg	−17,726.5	−0.0140	IBVS No.587
39006.5490	p	pg	−17,706	−0.0505	IBVS No.745
39060.4170	s	pg	−17,605.5	−0.0675	IBVS No.745
39361.5790	p	pg	−17,044	0.0355	IBVS No.587
39383.5070	p	ccd	−17,003	−0.0193	IBVS No.745
39404.3920	p	pg	−16,964	−0.0449	IBVS No.587
39414.3670	s	pg	−16,945.5	0.0108	IBVS No.587
39444.3590	s	pg	−16,889.5	−0.0225	IBVS No.587
39761.4910	p	pg	−16,298	−0.0346	IBVS No.587
39768.4830	p	ccd	−16,285	−0.0128	IBVS No.745
39771.4630	s	pg	−16,279.5	0.0182	IBVS No.587
40526.3910	s	pg	−14,871.5	0.0201	IBVS No.587
40530.3920	p	ccd	−14,864	−0.0001	IBVS No.745
40566.2850	p	ccd	−14,797	−0.0304	IBVS No.745
41261.7155	p	ccd	−13,500	−0.0112	IBVS No.745
41261.7176	p	ccd	−13,500	−0.0091	IBVS No.745
41261.7176	p	ccd	−13,500	−0.0091	IBVS No.745
41264.6664	s	ccd	−13,494.5	−0.0092	IBVS No.745
41264.6665	s	ccd	−13,494.5	−0.0091	IBVS No.745
41264.6687	s	ccd	−13,494.5	−0.0069	IBVS No.745
41268.6860	p	ccd	−13,487	−0.0109	IBVS No.745
41268.6866	p	ccd	−13,487	−0.0103	IBVS No.745
41268.6869	p	ccd	−13,487	−0.0100	IBVS No.745
41281.5561	p	ccd	−13,463	−0.0089	IBVS No.745
41281.5566	p	ccd	−13,463	−0.0084	IBVS No.745
41281.5571	p	ccd	−13,463	−0.0079	IBVS No.745
41315.6012	s	ccd	−13,399.5	−0.0105	IBVS No.745
41315.6012	s	ccd	−13,399.5	−0.0105	IBVS No.745
41315.6022	s	ccd	−13,399.5	−0.0095	IBVS No.745
41317.4810	p	ccd	−13,396	−0.0073	IBVS No.745
41330.6166	s	ccd	−13,371.5	−0.0078	IBVS No.890
41350.2490	p	vis	−13,335	0.0543	BBSAG No.5
41534.6210	p	vis	−12,991	−0.0158	BBSAG No.3
41563.8530	s	ccd	−12,936.5	−0.0050	IBVS No.745
41571.6470	p	vis	−12,922	0.0145	BBSAG No.5
41580.4580	s	vis	−12,905.5	−0.0212	BBSAG No.5
41581.5660	s	vis	−12,903.5	0.0143	BBSAG No.5
41582.6340	s	vis	−12,901.5	0.0100	BBSAG No.5
41585.5660	p	vis	−12,896	−0.0068	BBSAG No.5
41587.4480	s	vis	−12,892.5	−0.0014	BBSAG No.5
41603.5390	s	vis	−12,862.5	0.0044	BBSAG No.6
41607.8360	s	ccd	−12,854.5	0.0121	IBVS No.745
41609.4370	s	vis	−12,851.5	0.0045	BBSAG No.6
41616.4020	s	vis	−12,838.5	−0.0006	BBSAG No.6
41620.6640	s	ccd	−12,830.5	−0.0279	IBVS No.745
41623.3580	s	vis	−12,825.5	−0.0148	BBSAG No.6
41624.4540	s	vis	−12,823.5	0.0088	BBSAG No.6
41627.3770	p	vis	−12,818	−0.0171	BBSAG No.6
41630.6030	p	ccd	−12,812	−0.0081	IBVS No.745
41631.4140	s	vis	−12,810.5	−0.0013	BBSAG No.6
41645.3470	s	vis	−12,784.5	−0.0087	BBSAG No.6
41648.2890	p	vis	−12,779	−0.0156	BBSAG No.6
41649.3690	p	vis	−12,777	−0.0080	BBSAG No.6
41653.3790	s	vis	−12,769.5	−0.0192	BBSAG No.7
41657.4250	p	vis	−12,762	0.0054	BBSAG No.7
41664.3820	p	vis	−12,749	−0.0077	BBSAG No.7

Table 1
(Continued)

HJD (2400000+)	Type	Method	Epoch	$O-C$ (d)	References
41673.2360	s	vis	−12,732.5	−0.0005	BBSAG No.7
41699.2340	p	vis	−12,684	−0.0067	BBSAG No.7
41707.2810	p	vis	−12,669	−0.0022	BBSAG No.7
41722.2750	p	vis	−12,641	−0.0210	BBSAG No.8
41900.5760	s	vis	−12,308.5	0.0037	BBSAG No.11
41904.5890	p	vis	−12,301	−0.0045	BBSAG No.11
41908.5970	s	vis	−12,293.5	−0.0177	BBSAG No.11
41912.6400	p	vis	−12,286	0.0039	BBSAG No.11
41934.6100	p	vis	−12,245	−0.0089	BBSAG No.11
41942.6520	p	vis	−12,230	−0.0095	BBSAG No.11
41958.4760	s	vis	−12,200.5	−0.0024	BBSAG No.12
41976.4400	p	vis	−12,167	−0.0001	BBSAG No.12
41987.4090	s	vis	−12,146.5	−0.0226	BBSAG No.12
41997.3490	p	vis	−12,128	−0.0017	BBSAG No.12
42005.3840	p	vis	−12,113	−0.0092	BBSAG No.12
42008.3390	s	vis	−12,107.5	−0.0032	BBSAG No.12
42011.2870	p	vis	−12,102	−0.0041	BBSAG No.12
42015.3070	s	vis	−12,094.5	−0.0054	BBSAG No.12
42026.2970	p	vis	−12,074	−0.0068	BBSAG No.13
42027.3690	p	vis	−12,072	−0.0072	BBSAG No.13
42035.4070	p	vis	−12,057	−0.0117	BBSAG No.13
42074.2810	s	vis	−11,984.5	−0.0100	BBSAG No.13
42289.5590	p	vis	−11,583	−0.0039	BBSAG No.17
42289.5590	p	vis	−11,583	−0.0039	BBSAG No.17
42298.6750	p	vis	−11,566	−0.0027	BBSAG No.17
42301.6200	s	vis	−11,560.5	−0.0067	BBSAG No.17
42318.5050	p	vis	−11,529	−0.0110	BBSAG No.17
42361.4020	p	vis	−11,449	−0.0075	BBSAG No.18
42365.4200	s	vis	−11,441.5	−0.0108	BBSAG No.18
42396.2580	p	vis	−11,384	−0.0025	BBSAG No.19
42402.4130	s	vis	−11,372.5	−0.0135	BBSAG No.19
42404.2980	p	vis	−11,369	−0.0051	BBSAG No.19
42414.2030	s	vis	−11,350.5	−0.0192	BBSAG No.20
42448.2440	p	vis	−11,287	−0.0249	BBSAG No.21
42448.2580	p	vis	−11,287	−0.0109	BBSAG No.21
42452.2720	s	vis	−11,279.5	−0.0182	BBSAG No.21
42620.6290	s	vis	−10,965.5	−0.0183	BBSAG No.23
42627.6030	s	vis	−10,952.5	−0.0145	BBSAG No.23
42710.4440	p	vis	−10,798	−0.0116	BBSAG No.24
42739.3870	p	vis	−10,744	−0.0217	BBSAG No.24
42768.3570	p	vis	−10,690	−0.0049	BBSAG No.25
42774.2590	p	vis	−10,679	−0.0007	BBSAG No.25
42778.2640	s	vis	−10,671.5	−0.0170	BBSAG No.25
42782.3040	p	vis	−10,664	0.0016	BBSAG No.26
42786.2940	s	vis	−10,656.5	−0.0295	BBSAG No.26
43058.4320	p	vis	−10,149	0.0025	BBSAG No.30
43077.4680	s	vis	−10,113.5	0.0045	BBSAG No.30
43088.4550	p	vis	−10,093	0.0001	BBSAG No.31
43357.6050	p	vis	−9591	−0.0067	BBSAG No.34
43361.6360	s	vis	−9583.5	0.0029	BBSAG No.34
43409.6110	p	vis	−9494	−0.0091	BBSAG No.35
43500.2260	p	vis	−9325	−0.0067	BBSAG No.36
43515.2380	p	vis	−9297	−0.0074	BBSAG No.36
43735.6060	p	vis	−8886	−0.0049	BBSAG No.38
43743.6510	p	vis	−8871	−0.0025	BBSAG No.38
43749.5530	p	vis	−8860	0.0016	BBSAG No.38
43772.6010	p	vis	−8817	−0.0056	BBSAG No.39
43814.4250	p	vis	−8739	−0.0028	BBSAG No.40

Table 1
(Continued)

HJD (2400000+)	Type	Method	Epoch	$O-C$ (d)	References
43828.3620	p	vis	−8713	−0.0062	BBSAG No.40
43905.2950	s	vis	−8569.5	−0.0134	BBSAG No.41
44087.6040	s	vis	−8229.5	−0.0019	BBSAG No.44
44098.5850	p	vis	−8209	−0.0124	BBSAG No.44
44132.6310	s	vis	−8145.5	−0.0131	BBSAG No.45
44164.5420	p	vis	−8086	−0.0042	BBSAG No.45
44210.3910	s	vis	−8000.5	0.0022	BBSAG No.46
44212.2680	p	vis	−7997	0.0026	BBSAG No.46
44238.5531	p	pe	−7948	0.0155	IBVS No.2185
44454.6140	p	vis	−7545	0.0002	BBSAG No.49
44458.6180	s	vis	−7537.5	−0.0170	BBSAG No.49
44461.5950	p	vis	−7532	0.0110	BBSAG No.49
44484.6320	p	vis	−7489	−0.0072	BBSAG No.50
44506.6130	p	vis	−7448	−0.0091	BBSAG No.50
44526.4520	p	vis	−7411	−0.0084	BBSAG No.51
44555.4160	p	vis	−7357	0.0024	BBSAG No.51
44583.3120	p	vis	−7305	0.0176	BBSAG No.52
44591.3310	p	vis	−7290	−0.0058	BBSAG No.52
44595.3500	s	vis	−7282.5	−0.0081	BBSAG No.52
44598.3110	p	vis	−7277	0.0039	BBSAG No.52
44602.3170	s	vis	−7269.5	−0.0113	BBSAG No.52
44613.3170	p	vis	−7249	−0.0027	BBSAG No.52
44627.2560	p	vis	−7223	−0.0041	BBSAG No.52
44635.2930	p	vis	−7208	−0.0097	BBSAG No.52
44831.5360	p	vis	−6842	−0.0046	BBSAG No.56
44842.5300	s	vis	−6821.5	−0.0020	BBSAG No.56
44847.6240	p	vis	−6812	−0.0016	BBSAG No.56
44873.6120	s	vis	−6763.5	−0.0178	BBSAG No.56
44883.5520	p	vis	−6745	0.0029	BBSAG No.57
44924.2990	p	vis	−6669	0.0011	BBSAG No.57
44932.3370	p	vis	−6654	−0.0034	BBSAG No.57
45180.5540	p	vis	−6191	−0.0327	BBSAG No.61
45214.6270	s	vis	−6127.5	−0.0064	BBSAG No.59
45224.5540	p	vis	−6109	0.0014	BBSAG No.62
45231.5270	p	vis	−6096	0.0042	BBSAG No.62
45247.6070	p	vis	−6066	−0.0008	BBSAG No.63
45247.6090	p	vis	−6066	0.0011	BBSAG No.63
45249.4920	s	vis	−6062.5	0.0075	BBSAG No.63
45252.4230	p	vis	−6057	−0.0103	BBSAG No.63
45263.4170	s	vis	−6036.5	−0.0078	BBSAG No.63
45277.3710	s	vis	−6010.5	0.0057	BBSAG No.64
45323.2120	p	vis	−5925	0.0043	BBSAG No.64
45328.2920	s	vis	−5915.5	−0.0092	BBSAG No.64
45335.2530	s	vis	−5902.5	−0.0184	BBSAG No.64
45346.2600	p	vis	−5882	−0.0029	BBSAG No.64
45353.2340	p	vis	−5869	0.0008	BBSAG No.64
45357.2540	s	vis	−5861.5	−0.0004	BBSAG No.64
45536.5960	p	vis	−5527	−0.0069	BBSAG No.67
45540.5960	s	vis	−5519.5	−0.0282	BBSAG No.67
45543.5610	p	vis	−5514	−0.0121	BBSAG No.67
45566.6150	p	vis	−5471	−0.0134	BBSAG No.68
45585.6500	s	vis	−5435.5	−0.0124	BBSAG No.68
45594.5090	p	vis	−5419	−0.0002	BBSAG No.68
45596.6550	p	vis	−5415	0.0011	BBSAG No.69
45624.5370	p	vis	−5363	0.0022	BBSAG No.69
45634.4500	s	vis	−5344.5	−0.0038	BBSAG No.69
45659.3880	p	vis	−5298	0.0022	BBSAG No.69
45680.2970	p	vis	−5259	0.0006	BBSAG No.70

Table 1
(Continued)

HJD (2400000+)	Type	Method	Epoch	$O-C$ (d)	References
45691.2740	s	vis	−5238.5	−0.0137	BBSAG No.70
45702.2780	p	vis	−5218	−0.0012	BBSAG No.70
45705.2330	s	vis	−5212.5	0.0048	BBSAG No.70
45903.5920	s	vis	−4842.5	−0.0187	BBSAG No.73
45913.5420	p	vis	−4824	0.0121	BBSAG No.73
45914.6020	p	vis	−4822	−0.0002	BBSAG No.73
45917.5510	s	vis	−4816.5	−0.0001	BBSAG No.73
45921.5770	p	vis	−4809	0.0046	BBSAG No.73
46266.5900	s	vis	−4165.5	−0.0072	BBSAG No.77
46307.6240	p	vis	−4089	0.0098	BBSAG No.78
46427.1800	p	vis	−3866	0.0001	BBSAG No.79
46428.2520	p	vis	−3864	−0.0002	BBSAG No.79
46629.5780	s	vis	−3488.5	−0.0056	BBSAG No.80
46659.6170	s	vis	−3432.5	0.0078	BBSAG No.81
46749.4270	p	vis	−3265	0.0095	BBSAG No.82
46765.2470	s	vis	−3235.5	0.0125	BBSAG No.82
46798.2160	p	vis	−3174	0.0071	BBSAG No.82
47007.5800	s	vis	−2783.5	−0.0029	BBSAG No.84
47055.5800	p	vis	−2694	0.0099	BBSAG No.85
47097.3860	p	vis	−2616	−0.0052	BBSAG No.86
47169.2400	p	vis	−2482	0.0021	BBSAG No.87
47411.5940	p	vis	−2030	0.0076	BBSAG No.89
47461.4620	p	vis	−1937	0.0119	BBSAG No.90
47547.2410	p	vis	−1777	0.0038	BBSAG No.91
47740.5350	s	vis	−1416.5	0.0089	BBSAG No.92
47854.4510	p	vis	−1204	−0.0110	BBSAG No.93
48123.6270	p	vis	−702	0.0081	BBSAG No.96
48255.2720	s	vis	−456.5	0.0235	BBSAG No.97
48470.5380	p	vis	−55	0.0177	BBSAG No.98
48500.0118	p	ccd	0	0.0022	Paschke A.(Hipparcos)[a]
48543.4360	p	vis	81	−0.0032	BBSAG No.99
48845.5640	s	vis	644.5	−0.0065	BBSAG No.102
49026.2500	s	vis	981.5	−0.0095	BBSAG No.103
49313.3750	p	vis	1517	−0.0031	BBSAG No.105
49705.3180	p	vis	2248	0.0002	BBSAG No.108
49983.5840	p	vis	2767	−0.0055	BBSAG No.110
49990.5330	p	vis	2780	−0.0266	BBSAG No.113
50423.2440	p	vis	3587	−0.0041	BBSAG No.114
50672.5680	p	vis	4052	0.0012	BBSAG No.115
50823.2310	p	vis	4333	0.0006	BBSAG No.117
51058.5950	p	vis	4772	−0.0135	BBSAG No.119
51095.0690	p	ccd	4840	0.0009	VSOLJ No.33
51095.0690	p	ccd	4840	0.0009	VSOLJ No.47
51513.2690	p	vis	5620	−0.0109	BBSAG No.121
51557.2270	p	vis	5702	−0.0188	BBSAG No.122
52214.5800	p	ccd	6928	−0.0091	Paschke A. (ASAS)[a]
52218.3440	p	vis	6935	0.0016	BBSAG No.127
52620.9920	p	vis	7686	−0.0133	VSOLJ No.817
52634.9350	p	vis	7712	−0.0106	VSOLJ No.817
52636.0100	p	vis	7714	−0.0080	VSOLJ No.817
52924.4680	p	vis	8252	−0.0090	BBSAG No.130
52990.9610	p	vis	8376	−0.0009	VSOLJ No.1163
53012.9290	p	vis	8417	−0.0159	VSOLJ No.1202
53252.6160	p	vis	8864	0.0034	OEJV No.3
53296.0420	p	vis	8945	−0.0002	VSOLJ No.0043
53319.0680	p	vis	8988	−0.0294	VSOLJ No.0043
53324.9690	p	vis	8999	−0.0263	VSOLJ No.0043
53333.0220	p	vis	9014	−0.0158	VSOLJ No.0043

Table 1
(Continued)

HJD (2400000+)	Type	Method	Epoch	$O-C$ (d)	References
53682.0570	p	vis	9665	−0.0269	VSOLJ No.0044
53687.4389	p	ccd	9675	−0.0067	IBVS No.6153
53704.0560	p	vis	9706	−0.0108	VSOLJ No.0044
53738.9123	p	ccd	9771	−0.0055	VSOLJ No.0045
54024.1560	p	vis	10,303	−0.0038	VSOLJ No.0045
54040.7756	p	ccd	10,334	−0.0054	IBVS No.5843
54052.0100	p	vis	10,355	−0.0306	VSOLJ No.0045
54394.0960	p	vis	10,993	−0.0205	VSOLJ No.0046
54416.0810	p	vis	11,034	−0.0184	VSOLJ No.0046
56609.0248	p	pg	15,124	−0.0062	VSOLJ No.0056
56615.9875	p	pg	15,137	−0.0137	VSOLJ No.0056
56637.9740	p	pg	15,178	−0.0102	VSOLJ No.0056
56640.9154	s	pg	15,183.5	−0.0177	VSOLJ No.0056
56641.9798	s	pg	15,185.5	−0.0256	VSOLJ No.0056
56648.9579	s	pg	15,198.5	−0.0177	VSOLJ No.0056
56955.1168	s	pg	15,769.5	−0.0114	VSOLJ No.0059
56974.9535	s	pg	15,806.5	−0.0129	VSOLJ No.0059
56996.9345	s	pg	15,847.5	−0.0149	VSOLJ No.0059
58386.1464	s	TESS	18,438.5	−0.0171	This Paper
58386.4136	p	TESS	18,439	−0.0180	This Paper
58392.0446	s	TESS	18,449.5	−0.0168	This Paper
58392.3121	p	TESS	18,450	−0.0173	This Paper
58401.1583	s	TESS	18,466.5	−0.0179	This Paper
58401.4271	p	TESS	18,467	−0.0172	This Paper
59116.1379	p	TESS	19,800	−0.0198	This Paper
59116.4064	s	TESS	19,800.5	−0.0194	This Paper
59126.0573	s	TESS	19,818.5	−0.0196	This Paper
59126.3255	p	TESS	19,819	−0.0194	This Paper
59136.2446	s	TESS	19,837.5	−0.0195	This Paper
59136.5120	p	TESS	19,838	−0.0202	This Paper
59141.0703	s	TESS	19,846.5	−0.0193	This Paper
59141.3375	p	TESS	19,847	−0.0202	This Paper

Note.
[a] The data from $O-C$ gateway, http://var2.astro.cz/ocgate/.

The parameters and errors derived from the $O-C$ analysis are presented in Table 3, and the $O-C$ graph is displayed in Figure 3. Looking at the data distribution of about 60 yr, it is seen that the OP of AA Cet shows a constantly decreasing change (see Figure 3). The OP decrease of AA Cet has been calculated at 0.62 ± 0.06 s per century, and the reason for this can be suggested as conservative mass transfer between components.

5. Results and Discussion

There is no LC analysis related to the AA Cet system in the literature. The LC obtained from TESS data for AA Cet was analyzed by the WD method, and the physical parameters of the system were obtained. In the analysis, photometric data were combined with the RV data obtained by Duerbeck & Rucinski (2007). The absolute parameters of the components of AA Cet were calculated by basic astrophysical equations using parameters obtained from simultaneous analyses of light and RV curves (see Table 4). The temperature difference between the components was calculated as 1305 K, and the system may not have reached thermal equilibrium. The degree of contact of AA Cet was calculated to be $f = 8\%$, and it was seen that it has a marginal contact of type A. The mass ratio of AA Cet was obtained as $q = 0.347 \pm 0.008$, which supports the value of $q = 0.35 \pm 0.02$ calculated by Duerbeck & Rucinski (2007). While calculating the absolute parameters for AA Cet, the values for the Sun determined by Pecaut & Mamajek (2013) were used ($T_{\mathrm{eff}\odot} = 5771.8(7)$ K, $M_{\mathrm{bol}\odot} = 4.7554(4)$ mag, $g_\odot = 27423.2(7.9)$ cm s^{-2}). Bolometric correction (BC) values for the components were reported by Eker et al. (2020) and are given in Table 4. For AA Cet, the masses and radii of the components were calculated as $M_1 = 1.39 \pm 0.04$ $M_\odot$, $M_2 = 0.48 \pm 0.02$ $M_\odot$ and $R_1 = 1.64 \pm 0.03$ $R_\odot$, $R_2 = 1.01 \pm 0.04$ $R_\odot$, respectively. The photometric distance of the system

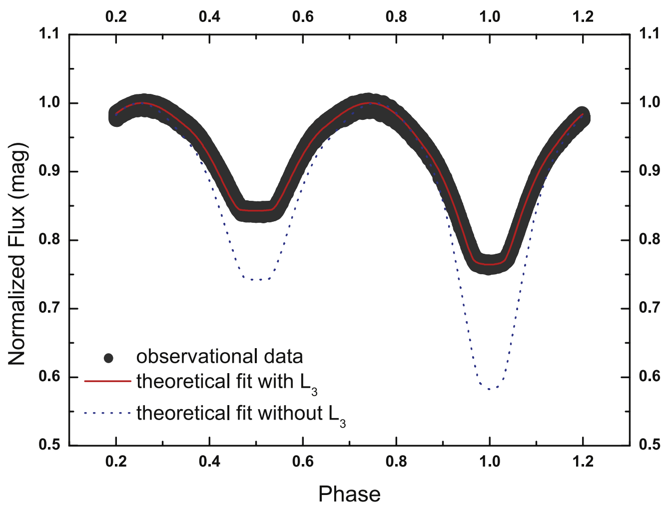

Figure 1. The best theoretical fit for AA Cet's TESS LC.

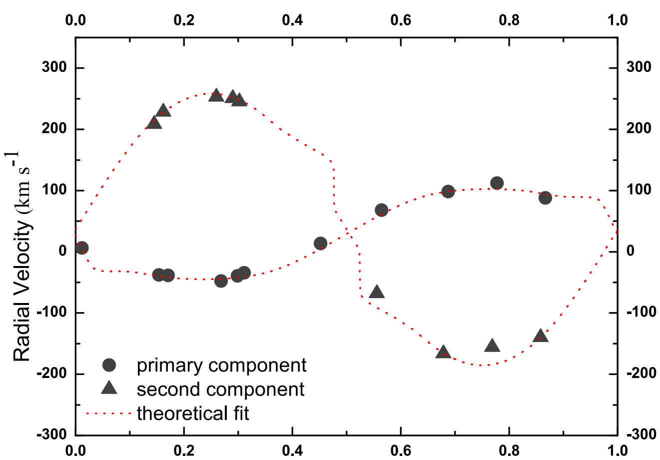

Figure 2. Comparison of RV data for components of AA Cet with theoretical curves.

was calculated as 94 ± + 6 pc, and this value is consistent with the value from Gaia Data Release 3 (DR3, Gaia Collaboration 2022) (see Table 4). Since the AA Cet system is a member of a visual binary, the third light contribution value was determined to be approximately 41%. The ratio of apparent luminosities determined from the broadening functions are estimated as $l_3/(l_1 + l_2) = 0.59$ by Pribulla & Rucinski (2006). The value we obtained (approximately 0.68) was slightly larger than their estimated value.

An OP analysis of AA Cet with 264 eclipse times (ccd = 32, pe = 1, pg = 21, vis = 196 and TESS = 14) spanning approximately 60 yr was performed for the first time. It has been observed that the OP of AA Cet has decreased, and especially the eclipse times calculated in this study support this decrease. For AA Cet, the OP decrease rate was calculated as $dP/dt = 7.2(7) \times 10^{-8}$ d yr^{-1}. The reason for this decrease

Table 2
Parameters and Their Errors found from Simultaneous Analysis of Light and RV Curves of AA Cet

Parameter	AA Cet
i (°)	84.05 (35)
T_1(K)	6500
T_2(K)	5195 (32)
$\Omega_1 = \Omega_2$	2.548 (21)
q	0.347 (8)
$a(R_\odot)$	3.42 (20)
V_γ (km s^{-1})	35 (1)
$L_1/(L_{\rm tot.})$	0.500 (3)
$L_2/(L_{\rm tot.})$	0.095
$L_3/(L_{\rm tot.})$	0.405 (4)
r_1(pole)	0.4479 (5)
r_1(side)	0.4805 (9)
r_1(back)	0.5076 (6)
r_2(pole)	0.2751 (8)
r_2(side)	0.2871 (8)
r_2(back)	0.3224 (7)
f (%)	8

Note. $^*T_1$ was determined from the spectral type.

has been suggested as mass (and energy) transfer between components with the assumption of conservative mass. This rate was calculated as $dM/dt = 3.3(9) \times 10^{-8}$ $M_\odot$ yr^{-1} from the more massive component to the less massive one. The decrease in OPs of eclipsing systems may be due to either conservative mass transfer between components or angular momentum loss (AML) of the systems. There is no evidence of magnetic activity for AA Cet both in this study and in the literature. Many authors have stated that the reason for the decrease in OPs of CBs may be due to TRO or TRO+AML (e.g., Qian 2001a, 2001b, 2003; Yıldırım 2023). Therefore, the OP variation of AA Cet can also be explained by TRO. As a result of the LC analysis, the value of third light contribution (l_3) was obtained to be approximately 41%, but no sinusoidal change was observed in the OP analysis. AA Cet and SAO 167450 are members of the visual binary system. Both members of this visual binary are also binary systems and the system is quadruple in total (Fekel & Willmarth 2009). The light contribution of SAO 167450 was determined as l_3 in LC analysis because this visual member is located only 8″ from AA Cet (Table 2). The magnitude difference in V filter between AA Cet and its visual companion SAO 167450 is only 0.33 mag (Perryman et al. 1997). Considering this value, the l_3/l_1 ratio (light ratio between the primary component of AA Cet and SAO 167450) in V filter can be estimated to over 0.80, which agrees with the l_3/l_1 value found in the TESS LC solution (Table 2). On the other hand, a sinusoidal change would be very difficult to observe in the OP analysis because the OP of the visual binary is very long (Fekel & Willmarth 2009).

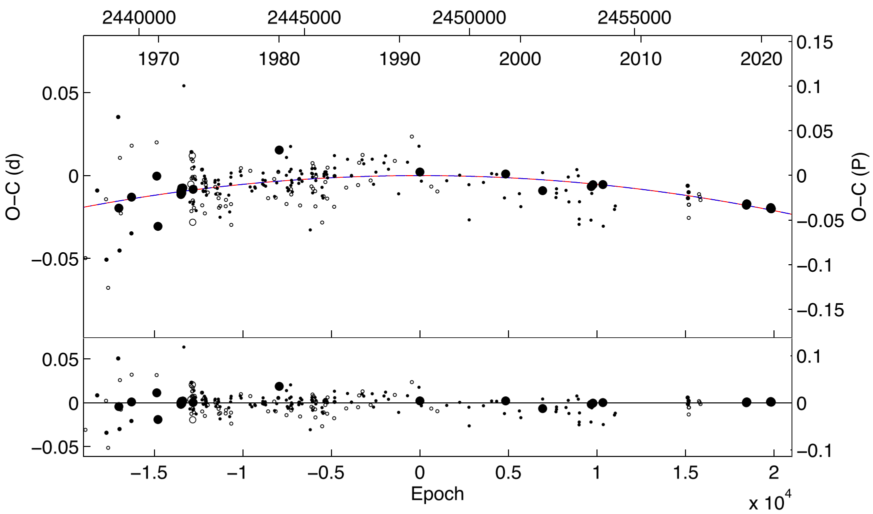

Figure 3. $O - C$ graph of AA Cet and the best theoretical parabolic fit representing the $O - C$ variations.

Table 3
The Parameters and Errors Derived from the $O - C$ Analysis of AA Cet

Parameter	AA Cet
T_0 (HJD+2400000)	48,500.0096 (5)
$P_{\rm orb}$ (day)	0.5361691 (7)
Q (day)	$0.53(5) \times 10^{-10}$
dP/dt (day yr^{-1})	$7.2(7) \times 10^{-8}$
dM/dt ($M_\odot$ yr^{-1})	$3.3(9) \times 10^{-8}$

Table 4
Basic Physical Parameters and Errors of AA Cet

Parameter	AA Cet
$M_1(M_\odot)$	1.39 (4)
$M_2(M_\odot)$	0.48 (2)
$R_1(M_\odot)$	1.64 (3)
$R_2(M_\odot)$	1.01 (4)
logg_1 (cgs)	4.15 (1)
logg_2 (cgs)	4.12 (18)
$M_{\rm bol,1}$ (mag)	3.17 (17)
$M_{\rm bol,2}$ (mag)	5.20 (23)
$L_1(L_\odot)$	4.27 (41)
$L_2(L_\odot)$	0.66 (12)
BC$_1$	0.070
BC$_2$	−0.178
$d_{\rm photometric}$(pc)	94 (7)
$d_{\rm Gaia-DR3}$(pc)	86 (2)

Since the systems with a low degree of contact are not in thermal equilibrium, the temperature difference between the components becomes larger than normal. The AA Cet system is most likely not in thermal equilibrium, and several systems similar to AA Cet have been selected from the literature and are listed in Table 5. In terms of OPs and degrees of contact, the selected systems show similar characteristics to AA Cet. Depending on the absolute parameters calculated for AA Cet, the locations of the components in the Hertzsprung–Russell (HR) diagram are shown in Figure 4. According to the Padova evolution model (Bressan et al. 2012), the log $T_{\rm eff}$−log L graph for the systems in AA Cet and Table 5 is displayed in Figure 4 (for $Z = 0.014$). In this diagram, the positions of the systems in Table 5 are also plotted to compare the position of AA Cet. According to the HR diagram, the second components seem to have evolved and left the main sequence, while the primary components are located on the main sequence. The secondary component of AA Cet is located closer to the Terminal Age Main Sequence (TAMS), unlike the secondary components of other systems.

A method based on the initial masses of the systems has been proposed by Yıldız (2014) to calculate the ages of CBs. The kinematic ages calculated for the CBs and the age calculation based on the initial masses are quite compatible with each other (Bilir et al. 2005; Yıldız 2014). The mean ages of A and W subtypes of CBs were calculated by Yıldız (2014) as 4.4 and 4.6 Gyr, respectively. The kinematic age of the CBs was determined as 5.47 Gyr by Bilir et al. (2005). The age of the marginal CB AA Cet was estimated to be 7 Gyr using the method proposed by Yıldız (2014) and used by Latkovic et al. (2021).

As a result, LC and OP analyses of the marginal CB AA Cet were performed in this paper. The basic physical parameters of AA Cet and the results of OP variation were presented for the first time to the literature. In this respect, this study will contribute to the literature in terms of both data and results. In future studies, precise spectral and photometric observation analyses will make significant contributions to our understanding of the nature and evolution of the system. In

Table 5
Some Information about a Few Marginal CBs Selected from the Literature

System	Period (day)	Degree of Contact (f %)	Spectral Type	ΔT (K)	$O-C$ Type	Reference
SZ Hor	0.625118	18	F3V	1698	Downward Par.	Duerbeck & Rucinski (2007), Deb & Singh (2011) Kreiner (2004)
TT Cet	0.485954	8	F4V	1535	Downward Par.	Duerbeck & Rucinski (2007), Kreiner (2004)
BX And	0.610112	4.5	F2V	1892	Downward Par. +Sinusoidal	Siwak & Zola (2010), Kreiner (2004)

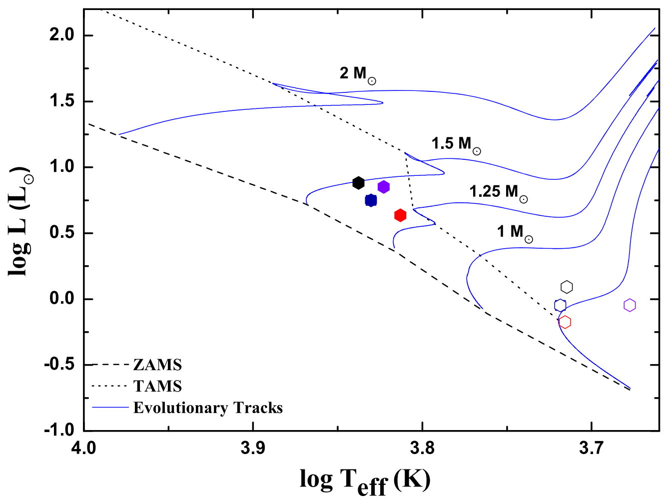

Figure 4. Positions of the components of AA Cet (red), SZ Hor (black), TT Cet (royal blue) and BX And (violet) in log T_{eff}–log L diagram. Evolutionary tracks, and Zero Age Main Sequence (ZAMS) and TAMS lines are drawn according to the Padova evolution model (Bressan et al. 2012). The solid hexagons in the diagrams are their primary components; the hollow hexagons represent their secondary components.

particular, studies on the other member of the visual binary will be very important in understanding the nature of this system.

Acknowledgments

We thank the referee for his/her suggestions and contributions. This work has made use of data from the European Space Agency (ESA) mission Gaia (https://www.cosmos.esa.int/gaia), processed by the Gaia Data Processing and Analysis Consortium (DPAC, https://www.cosmos.esa.int/web/gaia/dpac/consortium). Funding for the DPAC has been provided by national institutions, in particular the institutions participating in the Gaia Multilateral Agreement. This research has made use of the SIMBAD database, operated at CDS, Strasbourg, France. This paper includes data collected by the TESS mission. Funding for the TESS mission is provided by the NASA Science Mission Directorate. The MAST, Atlas $O-C$ and $O-C$ gateway databases were used in this paper. Thus, we express our gratitude to the working groups of MAST, Atlas $O-C$ and $O-C$ gateway.

References

Bilir, S., Karataş, Y., Demircan, O., & Eker, Z. 2005, MNRAS, 357, 497
Binnendijk, L. 1970, Vis. Astr., 12, 217
Bloomer, R. 1971a, IBVS, 586, 1
Bloomer, R. 1971b, IBVS, 587, 1
Bloomer, R. 1972, IBVS, 745, 1
Bressan, A., Marigo, P., Girardi, L., et al. 2012, MNRAS, 421, 127
Chambliss, C. R. 1981, IBVS, 2058, 1
Deb, S., & Singh, H. P. 2011, MNRAS, 412, 1787
Duerbeck, H. W., & Rucinski, S. M. 2007, AJ, 133, 169
Eker, Z., Soydugan, F., Bilir, S., et al. 2020, MNRAS, 496, 3887
Fekel, F. C., & Willmarth, D. W. 2009, PASP, 121, 1359
Flannery, B. P. 1976, ApJ, 205, 217
Gaia Collaboration 2022, yCat, I/355
Gazeas, K., & Stepien, K. 2008, MNRAS, 390, 1577
Kreiner, J. M. 2004, AcA, 54, 207
Latkovic, O., Ceki, A., & Lazarevic, S. 2021, MNRAS, 254, 18
Lucy, L. B. 1967, ZA, 65, 89
Lucy, L. B. 1976, ApJ, 205, 208
Paschke, A., & Brat, L. 2006, OEJVS, 23, 13
Pecaut, M. J., & Mamajek, E. E. 2013, ApJS, 208, 9
Perryman, M. A. C., Lindegren, L., Kovalevsky, J., et al. 1997, A&A, 323, L49
Pourbaix, D., Tokovinin, A. A., Batten, A. H., et al. 2004, A&A, 424, 727
Pribulla, T., & Rucinski, S. M. 2006, AJ, 131, 2986
Pribulla, T., Rucinski, S. M., Blake, R. M., et al. 2009, AJ, 137, 3655
Qian, S. B. 2001a, MNRAS, 328, 635
Qian, S. B. 2001b, MNRAS, 328, 914
Qian, S. B. 2003, MNRAS, 342, 1260
Ricker, G. R., Winn, J. N., Vanderspek, R., et al. 2015, JATIS, 1, 014003
Rucinski, S. M. 1969, AcA, 19, 245
Siwak, M., Zola, S., & Koziel, W. D. 2010, AcA, 60, 305
van Hamme, W. 1993, AJ, 106, 2096
van Hamme, W., & Wilson, R. E. 2003, ACP, 298, 323
Wilson, R. E., & Devinney, E. J. 1971, ApJ, 166, 605
Yıldırım, M. F. 2023, NewA, 99, 101946
Yıldız, M. 2014, MNRAS, 437, 185
Zhang, X. D., Qian, S. B., & Liao, W. P. 2020, MNRAS, 492, 4112